Turkish Journal of Electrical Engineering & Computer Sciences

http://journals.tubitak.gov.tr/elektrik/

Research Article

Turk J Elec Eng & Comp Sci
(2021) 29: 1736 – 1750
© TÜBİTAK
doi:10.3906/elk-2006-68

Power-based modelling and control: experimental results on a cart-pole double inverted pendulum

Tuğçe YAREN*, **Selçuk KİZİR**
Department of Mechatronics Engineering, Faculty of Engineering, Kocaeli University, Kocaeli, Turkey

Received: 12.06.2020 • **Accepted/Published Online:** 14.12.2020 • **Final Version:** 31.05.2021

Abstract: This paper is concerned with the modeling framework based on power and control for a mechanical system that has nonlinear, unstable, and under-actuated characteristic features, based on an analogy, which is developed by using the Brayton and Moser's (BM) equations between mechanical and electrical systems. The analogy is based on a mixed-potential function generalized for BM. The mixed-potential function for a cart - pole double inverted pendulum (CPDIP) system is used as a new building block for modeling, analysis, and controller design. The analogy allows for the exact transfer of results from electrical circuit synthesis and analysis to the mechanical domain. This paper focuses mainly on the development of the electrical equivalent circuit of CPDIP inspired by the power-based modeling framework. In this brief, a real time CPDIP experimental setup was modeled by using this framework and a linear quadratic regulator (LQR) controller was designed for the stabilization of the system. Experimental results validated that this framework can be used as a new and advantageous modeling method and is a convenient and practical alternative to the Lagrangian framework.

Key words: Analogy, Brayton–Moser, double inverted pendulum, linear quadratic regulator, optimal control, real time control

1. Introduction

The Euler–Lagrange (EL) or Hamiltonian method can describe a wide range class of physical systems [1–3]. Based on the energy balance of the system, one can systematically provide the equations of motion for both sets of equations [4]. In addition to energy-based methods, Brayton–Moser (BM) equations can describe a system in the power-based framework [5, 6].

Brayton and Moser developed a specific gradient form in the early 1960s to describe a wide range class of nonlinear electric networks [7–9]. The BM equations are based on the mixed-potential function that consists of a supplementary term that indicates the difference between content and cocontent functions, as well as the instantaneous transfer of power between subsystems [10–12]. Consequently, the BM equations are a modeling framework based on power since the mixed-potential is a power function [13]. In electrical systems, the inductor currents and capacitor voltages are basic variables and can be easily measured. Therefore, it is an important advantage that the system's dynamics can be defined in terms of these variables [14]. Since BM equations provide this advantage, an analogy between mechanical and electrical systems can be developed based on the BM equations [15]. Dirksz and Scherpen [8] proposed an integral control scheme for a standard mechanical system based on the power-based modeling framework. The proposed controller was implemented on a real-

*Correspondence: tugce.yaren@kocaeli.edu.tr

This work is licensed under a Creative Commons Attribution 4.0 International License.

time planar manipulator setup. Rinaldis and Scherpen [15] presented an electrical explanation that conforms to the BM concept of mechanical systems moving such as single, double pendulum, and single link inverted pendulum in the plane. The starting point was given by the Euler–Lagrange equations. Then, by inserting the pseudo-inductor, the BM equations for mechanical systems were determined. Jeltsema and Scherpen [16] showed that a wide range class of mechanical systems can be identified by a homonymous set of BM equations. In [16], the aim is to rewrite the standard Hamiltonian motion equations in terms of a power-based definition and they weren't looking for a exact electrical explanation.

The inverted pendulum (IP) system is an under-actuated system that has nonlinear and unstable characteristic features and also it is one of the most widely preferred testbed systems in control theory applications. Therefore, many IP systems that have different structure have been designed such as Pendubot, Acrobot, spherical/mobile/rotary/wheeled and single or multiple link IP [17, 18]. If the number of the link is increased, the control problem of the IP system that has two basic routines as stabilization and swing-up will be more difficult. In this study, the stabilization control problem is focused on, and the aim is to control the pendulum angles and the cart position at the upper unstable equilibrium point. There are many different studies in the literature on this control problem and Euler–Lagrange formulation is used for the modeling in most of them [19–21].

This paper aims to develop an optimal feedback control algorithm by using power-based modelling based on the BM framework for the stabilization problem of the cart - pole double inverted pendulum (CPDIP) in real time. Our main motivation is to develop an electrical interpretation of the CPDIP, which is a nonlinear and unstable mechanical system. Our power-based description form of mechanical systems is an electrical equivalent circuit. By using this form, a linear quadratic regulator (LQR) controller is designed and implemented on the real time cart – pole double inverted pendulum system. Experimental results are presented for optimal LQR control of a CPDIP under different conditions such as applying measurement noise and external disturbance. Determination of LQR parameters was readdressed and the process of tuning of the six controller gains was analyzed. The main contribution of this paper is development of electrical equivalent circuit of cart – pole double inverted pendulum inspired by the power-based modeling framework. We focus on a new and advantageous modelling method for controller design of CPDIP system and suggest the BM equations as a convenient and practical alternative to the Lagrangian framework. Also, the controller based on power based modelling is applied on an experimental CPDIP setup.

This paper is organized as follows. Section 2 presents to mathematical modelling based on BM framework of the CPDIP system. Section 3 describes LQR design for CPDIP. In section 4, experimental setup and results are presented.

2. Mathematical modelling based on BM framework

The schematic diagram of the CPDIP system is shown in Figure 1. The positive sense of rotation is defined to be counter-clockwise (CCW), when facing the system and the positive direction of linear displacement of the cart is to the right when facing the cart as can be seen from figure. The cart has mass (m_0) and is actuated by an applied force, F which is the only input in CPDIP. The system-related parameters are outlined in Table 1.

The dynamic model of the system has been based on the BM framework. In the BM framework, Euler–Lagrange (EL) equations can be transformed into BM equations if all the necessary conditions are met [15]. Also, the BM equations obtained represent an electrical circuit. Thus, the electrical equivalent circuit of the CPDIP system is achieved.

EL equations are based on the difference between the potential energy and the kinetic energy of the system. The starting point of the EL method is the determination of the generalized coordinates (q_i and $\dot{q}_i$) of

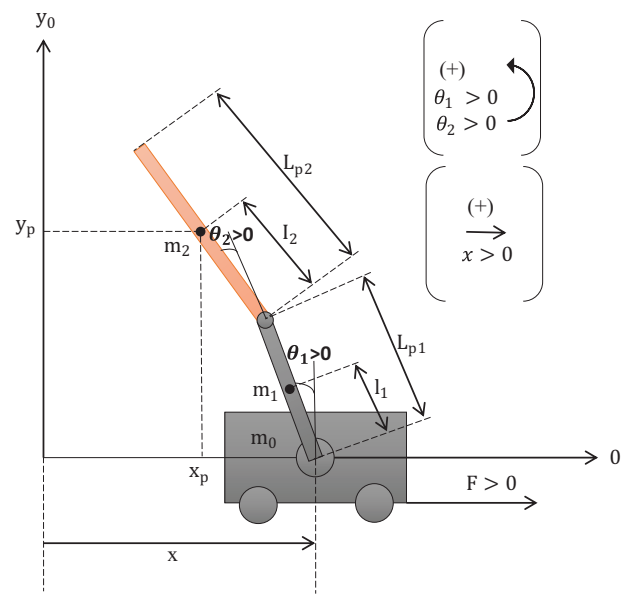

Figure 1. The schematic diagram of CPDIP.

Table 1. Parameters description of the CPDIP schematic diagram.

Parameter	Description of parameter
θ_1	The deflection angle between the first pendulum and the reference plane
θ_2	The deflection angle between the second pendulum and the first pendulum
x	The distance between the cart and the reference plane
m_0	Mass of the cart
m_1	Mass of the first pendulum
m_2	Mass of the second pendulum
l_1	Distance the mass center of the first pendulum to the corresponding joint
l_2	Distance the mass center of the second pendulum to the corresponding joint
L_{p1}	Length of the first pendulum
L_{p2}	Length of the second pendulum
g	Gravitational acceleration
F	Applied force to the system

the system and the m_i mass's position and velocity are describing these coordinates. According to the analogy approach, position, and velocity which are mechanical variables can be switched with the electrical variables and this switch leads to a series of equations for simple motion systems. If there are Coriolis and centrifugal terms in the motion equations, this system is no longer a simple motion system and the basic analogy approach can't be applied to these systems. However, [15] proposes conditions where the analogy approach is applicable even for complex mechanical behavior. Thus, the behavior of complex mechanical systems can be interpreted electrically by using the advanced analogy. The standard EL equations for a mechanical system are defined as

$$\frac{d}{dt}\left(\frac{\partial L(q,\dot{q})}{\partial \dot{q}}\right) - \frac{\partial L\left(q,\dot{q}\right)}{\partial q} = \tau \quad (q \in \mathbb{R}^r, \tau \in \mathbb{R}^r), \tag{1}$$

where r is the degree of freedom of the system and τ is external forces. Also, L is the Lagrangian function that is defined as

$$\mathrm{L}\left(\mathrm{q},\dot{\mathrm{q}}\right) \triangleq \mathrm{T}\left(\mathrm{q},\dot{\mathrm{q}}\right) - \widehat{\mathrm{V}}\left(\mathrm{q}\right), \tag{2}$$

where T is the kinetic energy of the system which is defined as following

$$\mathrm{T}\left(\mathrm{q},\dot{\mathrm{q}}\right) = \frac{1}{2}\dot{\mathrm{q}}^{\mathrm{T}}\mathrm{D}\left(\mathrm{q}\right)\dot{\mathrm{q}}. \tag{3}$$

$\hat{V}\left(q\right)$ is the potential function of the system and $D\left(q\right) \in \mathbb{R}^{rxr}$ is the mass matrix. For CPDIP system, generalized coordinates (q) and generalized torque vector (τ) are shown as:

$$q = \left[x\ \theta_1\ \theta_2\right],\ \tau = \left[\tau_1\ 0\ \ 0\right], \tag{4}$$

where x is the linear cart position, θ_1 is the bottom pendulum angle and θ_2 is the top pendulum angle as shown in Figure 1. Besides, since only torque is applied to the cart in the system, the first element of the torque vector is τ_1 and the other elements are zero. There is no torque available in the axis of θ_1 and θ_2, which are two passive joints. Although no torque normally is applied to pendulum joints, friction forces are applied to pendulum joints because of frictions that occur at joints and affect the performance of the controller. Therefore, friction forces are a critical part of dynamic systems and should be modeled as close as possible to the real system characteristics. In general, the friction forces are neglected. However, we considered to friction forces at pendulum joints in this paper. The linear expressions model the viscous friction forces at the joints:

$$F_{p1} = -b_1\dot{\theta_1} - b_2\left(\dot{\theta_1} - \dot{\theta_2}\right),\quad F_{p2} = -b_2\left(\dot{\theta_2} - \dot{\theta_1}\right), \tag{5}$$

where the parameters b_i denote the viscous friction coefficients at the respective joint i. Also, there is another friction force, which occurs between the cart and the rail in the system. This force is modeled as $c\dot{x}$ where the parameter c denotes the viscous friction coefficient. Therefore, generalized forces which consist of input force and friction forces in the system are $\Xi = \left[F - c\dot{x},\ F_{p1},\ F_{p2}\right]^T$.

V function is defined as

$$V\left(\theta\right) = K_1 cos\theta_1 + K_2 cos\theta_2, \tag{6}$$

where $K_1 = m_1 g l_1 + m_2 g L_{p1}$ and $K_2 = m_2 g l_2$. T is calculated in detail as following

$$T\left(\theta,\dot{\theta},\dot{x}\right) = \tfrac{1}{2}\left(D_{11}\dot{x}^2 + D_{22}\dot{\theta_1}^2 + D_{33}\dot{\theta_2}^2\right) + D_{12}\dot{x}\dot{\theta_1} + D_{13}\dot{x}\dot{\theta_2} + D_{23}\dot{\theta_1}\dot{\theta_2}, \tag{7}$$

where
$D_{11} = m_0 + m_1 + m_2,$
$D_{22} = m_1 {l_1}^2 + m_2 {L_{p1}}^2 + m_2 {l_2}^2 + 2m_2 L_{p1} l_2 cos\theta_2,$
$D_{33} = m_2 {l_2}^2,$
$D_{12} = D_{21} = -((m_1 l_1 + m_2 L_{p1})\, cos\theta_1 + m_2 l_2 \cos\left(\theta_1 + \theta_2\right)),$
$D_{13} = D_{31} = -m_2 l_2 cos(\theta_1 + \theta_2),$
$D_{23} = D_{32} = m_2 {l_2}^2 + m_2 L_{p1} l_2 cos\theta_2.$

In the analogy, the angular position θ corresponds to the charge stored in the capacitor q_p. The angular velocity $\dot{\theta}$ is related to the current vector $\mathrm{i_p}$ (replace $[\theta_1,\ \dot{\theta}_1,\ \theta_2,\ \dot{\theta}_2,\ \dot{x}]$ by $[q_{p1}, i_{p1},\ q_{p2},\ i_{p2},\ i_{p3}]$). Thus,

$$L\left(q_p, i_p\right) = \frac{1}{2}{i_p}^T D\left(q_p\right) i_p - \sum_{j=1}^{2} \int f_q^j\left(q_{pj}\right) dq_{pj}, \tag{8}$$

where $i_p = [i_{p1},\ i_{p2},\ i_{p3}]^T$. $q_p \in R^r$ is dependency of the general mass matrix $D(q_p)$ that can be expressed in terms of a new variable $q_\sigma \in R^s$ [15]. s is the amount of potential energy sources in system and it is equal 2 for CPDIP. Also, CPDIP is a *3* degrees of freedom (r) mechanical system. Therefore, $(s \neq r)$, a virtual potential energy source is added [15] and potential energy terms are expressed in terms of q_σ. Potential energy terms are

$$\begin{array}{l} \int f_q^1\left(q_{\sigma 1}\right) dq_{\sigma 1} = K_1 cos q_{\sigma 1}, \\ \int f_q^2\left(q_{\sigma 2}\right) dq_{\sigma 2} = K_2 cos q_{\sigma 2}. \end{array} \tag{9}$$

Virtual potential energy source is

$$\int f_v^3\left(v_{\sigma 3}\right) dv_{\sigma 3}, \quad f_v^3\left(v_{\sigma 3}\right) = C_3 v_{\sigma 3}, \tag{10}$$

where $v_\sigma \in R^s$ defines the voltages across the capacitors. Also, virtual potential energy source's energetic contribution is approximately zero. Assume that C_3 is very large so that

$$\lim_{C_3 \to \infty} \frac{1}{2C_3} {q_{\sigma 3}}^2 = 0. \tag{11}$$

The following relations can be derived from potential energy terms:

$$f_q^j\left(q_{\sigma j}\right) = K_j sin q_{\sigma j}, \quad j = 1, 2. \tag{12}$$

As far as they are locally invertible for $q_{\sigma j} \in \left(-\frac{\pi}{2}, \frac{\pi}{2}\right)$, naming $f_q^j\left(q_{\sigma j}\right) = -v_{\sigma j}$, we have that

$$q_{\sigma j} = \arcsin\left(-\frac{v_{\sigma j}}{K_j}\right) = -f_v^j\left(v_{\sigma j}\right),\ j = 1, 2, \tag{13}$$

and

$$\frac{\partial f_v^j\left(v_{\sigma j}\right)}{\partial v_{\sigma j}} = \frac{1}{\sqrt{K_j^2 - {v_{\sigma j}}^2}} = C_j\left(v_{\sigma j}\right), \tag{14}$$

are well defined in the open interval$(-K_j,\ K_j)$. With virtual capacitor [15], in terms of the Brayton–Moser framework, the Euler-Lagrange equations can be rewritten as follows:

$$-Q\left(i_p,\ v_\sigma\right) \left[\begin{array}{c} \frac{di_p}{d_t} \\ \frac{dv_\sigma}{dt} \end{array} \right] = \left[\begin{array}{c} \frac{\partial P(i_p, v_\sigma)}{\partial i_p} \\ \frac{\partial P(i_p, v_\sigma)}{\partial v_\sigma} \end{array} \right], \tag{15}$$

with

$$Q\left(i_p,\ v_\sigma\right) = \left[\begin{array}{cc} -\tilde{D}\left(v_\sigma\right) & (\bar{D}\left(i_p,\ v_\sigma\right) - \hat{D}(i_p,\ v_\sigma))C(v_\sigma) \\ 0 & C(v_\sigma) \end{array} \right], \tag{16}$$

and the functions $F(i_p)$ and $G(v_\sigma)$ are the content and the cocontent of the mixed potential function $P(i_p, v_\sigma)$,, respectively. Also with for ease of notation $f_v^j(v_{\sigma j}) = f_v^j$. For $i = 1, 2, 3$:

$$\begin{aligned}
&\tilde{D}_{ii}(v_\sigma) = D_{ii} \\
&\tilde{D}_{12}(v_\sigma) = -((m_1 l_1 + m_2 L_1) cos f_v^1 + m_2 l_2 \cos\left(f_v^1 + f_v^2\right)) \\
&\tilde{D}_{13}(v_\sigma) = -m_2 l_2 \cos\left(f_v^1 + f_v^2\right)) \\
&\tilde{D}_{23}(v_\sigma) = m_2 {l_2}^2 + m_2 L_1 l_2 cos f_v^2 \\
&\bar{D}_{ii}(i_p, v_\sigma) = \hat{D}_{ii}(i_p, v_\sigma) = 0 \\
&\bar{D}_{12}(i_p, v_\sigma) = ((m_1 l_1 + m_2 L_1) sin f_v^1 + \\
&m_2 l_2 \sin\left(f_v^1 + f_v^2\right)) i_{p1} + m_2 l_2 \sin\left(f_v^1 + f_v^2\right) i_{p2} \\
&\bar{D}_{13}(i_p, v_\sigma) = m_2 l_2 \sin\left(f_v^1 + f_v^2\right) i_{p1} + \\
&m_2 l_2 \sin\left(f_v^1 + f_v^2\right) i_{p2} \\
&\bar{D}_{23}(i_p, v_\sigma) = -m_2 L_1 l_2 sin f_v^2 i_{p2} \\
&\hat{D}_{12}(i_p, v_\sigma) = ((m_1 l_1 + m_2 L_1) sin f_v^1 + \\
&m_2 l_2 \sin\left(f_v^1 + f_v^2\right)) i_{p1} \\
&\hat{D}_{21}(i_p, v_\sigma) = m_2 l_2 \sin\left(f_v^1 + f_v^2\right) i_{p2} \\
&\hat{D}_{13}(i_p, v_\sigma) = m_2 l_2 \sin\left(f_v^1 + f_v^2\right) i_{p1} \\
&\hat{D}_{31}(i_p, v_\sigma) = m_2 l_2 \sin\left(f_v^1 + f_v^2\right) i_{p2} \\
&\hat{D}_{23}(i_p, v_\sigma) = 0,\ \hat{D}_{32}(i_p, v_\sigma) = -m_2 L_1 l_2 sin f_v^2 i_{p2}.
\end{aligned} \tag{17}$$

Furthermore, $v_\sigma = \left[-(m_1 + m_2) l_1 g sin f_v^1,\ m_2 l_2 g sin f_v^2\right]^T$ and $P(i_p, v_\sigma) = \tau^T i_p + {i_p}^T v_\sigma$. The torque vector τ is equivalent to the voltage source vector $E = [E_1,\ 0,\ 0]^T$. An explanation of this series of equations by the electrical view (17) is provided and can be depicted in Figure 2. In this figure, the subscript (i) for 1,2,3 represents the electrical variables of the cart, first pendulum and second pendulum, respectively. Thus, mechanical variables and components are expressed as electrical variables and components by using electrical interpretation within the BM form of mechanical systems moving in the plane in [15, 22].

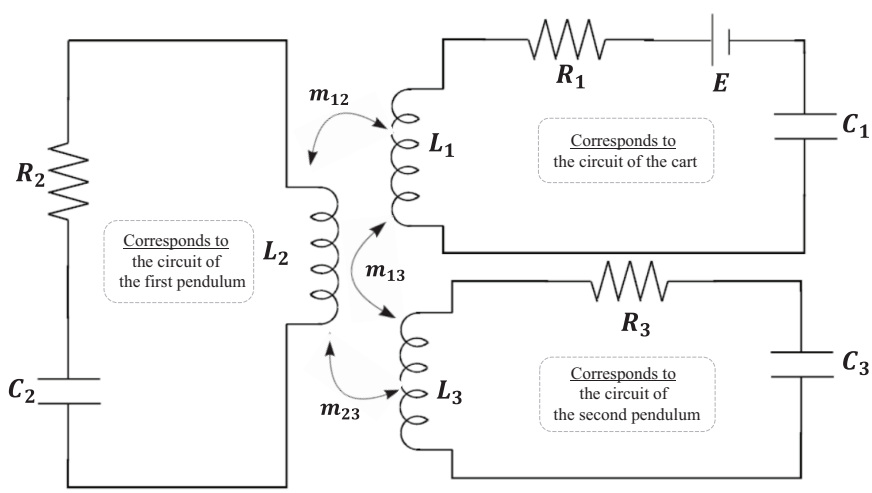

Figure 2. Equivalent electrical circuit of CPDIP.

Since there are three masses $(m_0,\ m_1,\ m_2)$ in the mechanical system, there are three inductances $(L_1,\ L_2,\ L_3)$ in the circuit. However, their analogies are different that the cart has translational, and the pendulums

have rotational motion. Therefore, by using the translational mechanical analogy L_1 can be determined as m_0. In a similar way, by using the rotational mechanical analogy, L_2 can be determined as $m_1 l_1{}^2$, and L_3 can be determined as $m_2 l_2{}^2$.

Since all masses in the system transfer their energy to each other, the inductors can be considered as three winding coupled inductors. However, the energy transfer between the cart and the second pendulum is indirect, while other energy transfers (the cart – the first pendulum, the first pendulum – the second pendulum) in the system are direct. Therefore, mutual inductance that exists between the cart and the second pendulum coils (m_{13}) is equal zero. The extent to which the mutual inductance m approaches the upper limit is specified by the coefficient of coupling k, given by [23]

$$m = k\sqrt{L_1 L_2}, \tag{18}$$

where $0 \leq k \leq 1$ or equivalently $0 \leq M \leq \sqrt{L_1 L_2}$. m_{12} is mutual inductance that exists between the cart and the first pendulum coils, m_{23} is mutual inductance that exists between the first and the second pendulum coils.

C_2, C_3 capacitance express the rotational forces in pendulums resulting from gravity, and C_1 is a virtual capacitor. C_2 can be determined as $1/(m_1 g l_1)$ and C_3 can be determined as $1/(m_2 g l_2)$ based on the simple harmonic motion. Since C_1 is virtual capacitor, assume that C_1 is very large.

R_1 is analogous to the viscous friction coefficient between the cart and the rail (c), R_i for 2, 3 is analogous to the viscous friction coefficient at the respective joint (b_i), respectively. Finally, all circuit elements can be seen from the Table 2.

Table 2. Elements description of the electrical circuit model of the CPDIP.

Parameter	Symbolic expression	Physical value
L_1	m_0	1.095 H
L_2	$m_1 l_1{}^2$	0.0025 H
L_3	$m_2 l_2{}^2$	0.0027 H
C_1	$\approx \infty$	10^9 F
C_2	$1/(m_1 g l_1)$	6.6388 F
C_3	$1/(m_2 g l_2)$	5.6651 F
R_1	c	0.001 Ω
R_2	b_1	0.000565 Ω
R_3	b_2	0.000072 Ω
m_{12}	$k_{12}\sqrt{L_1 L_2}$	0.0514
m_{13}	$k_{13}\sqrt{L_1 L_3}$	0
m_{23}	$k_{23}\sqrt{L_2 L_3}$	0.0026

In order to model the system, all electrical state variables must be obtained. Table 3 shows electrical state variables of the CPDIP system and their mechanical equivalent. The voltage and current equations related to the circuit in Figure 2 are given in (19) and (20). (19) is the voltage equations and (20) is the current equations.

$$V_{L1} = -V_{C1} - E + V_{R1}, \quad V_{L2} = -V_{C2} + V_{R2}, \quad V_{L3} = V_{C3} - V_{R3}, \tag{19}$$

$$i_{C1} = i_{L1} = -i_{R1}, \quad i_{C2} = i_{L2} = -i_{R2}, \quad i_{C3} = -i_{L3} = -i_{R3}. \tag{20}$$

Table 3. State variables of the CPDIP system.

Mechanical	Electrical
x	q_{c1}
$\dot{x}$	i_{L1}
θ_1	q_{c2}
$\dot{\theta}_1$	i_{L2}
θ_2	q_{c3}
$\dot{\theta}_2$	i_{L3}

The charge of the capacitor can be calculated as:

$$q = CV, \tag{21}$$

where C is the capacitance and V is the capacitor voltage. By taking account (19), (20) and (21) together, the state space model of electrical interpretation of the CPDIP is obtained as in (23). Define the matrix A as follows:

$$\begin{bmatrix} 0 & 0 & 0 & 1 & 0 & 0 \\ 0 & 0 & 0 & 0 & 1 & 0 \\ 0 & 0 & 0 & 0 & 0 & -1 \\ \frac{L_2L_3-m_{23}^2}{C_1Z} & \frac{m_{13}m_{23}-L_3m_{12}}{C_2Z} & \frac{L_2m_{13}-m_{12}m_{23}}{C_3Z} & \frac{R_1(L_2L_3-m_{23}^2)}{Z} & \frac{R_2(m_{13}m_{23}-L_3m_{12})}{Z} & \frac{R_3(m_{12}m_{23}-L_2m_{13})}{Z} \\ \frac{m_{13}m_{23}-L_3m_{12}}{C_1Z} & \frac{L_1L_3-m_{13}^2}{C_2Z} & \frac{L_1m_{23}-m_{12}m_{13}}{C_3Z} & \frac{R_1(m_{13}m_{23}-L_3m_{12})}{Z} & \frac{R_2(L_1L_3-m_{13}^2)}{Z} & \frac{R_3(m_{12}m_{13}-L_1m_{23})}{Z} \\ \frac{m_{12}m_{23}-L_2m_{13}}{C_1Z} & \frac{m_{12}m_{13}-L_1m_{23}}{C_2Z} & \frac{m_{12}^2-L_1L_2}{C_3Z} & \frac{R_1(m_{12}m_{23}-L_2m_{13})}{Z} & \frac{R_2(m_{12}m_{13}-L_1m_{23})}{Z} & \frac{R_3(L_1L_2-m_{12}^2)}{Z} \end{bmatrix}. \tag{22}$$

Then,

$$\frac{d}{dt}\begin{bmatrix} q_{c1} \\ q_{c2} \\ q_{c3} \\ i_{L1} \\ i_{L2} \\ i_{L3} \end{bmatrix} = A\begin{bmatrix} q_{c1} \\ q_{c2} \\ q_{c3} \\ i_{L1} \\ i_{L2} \\ i_{L3} \end{bmatrix} + \begin{bmatrix} 0 \\ 0 \\ 0 \\ \frac{L_2L_3-m_{23}^2}{Z} \\ \frac{m_{13}m_{23}-L_3m_{12}}{Z} \\ \frac{m_{12}m_{23}-L_2m_{13}}{Z} \end{bmatrix}, \tag{23}$$

where $Z = L_1m_{23}^2 + L_2m_{13}^2 + L_3m_{12}^2 - 2m_{12}m_{13}m_{23} - L_1L_2L_3$.

3. Optimal controller design

The designed controller of this system is to be able to drive the system output variables $(x,\ \theta_1,\ \theta_2)$ to the reference position $(x = 0\ m,\ \theta_1 = \theta_2 = 0^\circ)$ and maintain the stability of the system. The dynamic control performance of the system depends on the dynamic model of the system and efficiency of the control algorithm. Therefore, the exact parameterization of the model is a critical point for controller design of the CPDIP system. Directly measurable system parameters are determined as m_0=1.095 kg, m_1=0.096 kg, m_2=0.120 kg, l_1=0.160 m, l_2=0.150 m. Also, the moment of inertia Ji and friction coefficient for each pendulum arm must be determined. However, these parameters are not directly measurable. Therefore, they were obtained experimentally. In this paper, simple pendulum model is used to obtain friction coefficients. The procedure for deriving the equation of motion for the simple pendulum is similar to the one for the double pendulum, even

much easier. Thus, the unknown parameters are easily obtained. The motion equation of the simple pendulum is:

$$J\ddot{\theta} + mgl_c \sin\theta = -b\dot{\theta}, \tag{24}$$

where J is the moment of inertia of the pendulum, m is the the mass of the pendulum, b is the viscous friction coefficient, l_c is the distance of the center of gravity to the joint. There are two unknowns in (24), J and b. For CPDIP system, pendulums were analyzed separately and these parameters were identified by two experiments. First, the joint between the two pendulums was fixed. In this way, the whole pendulum acted as a simple pendulum. Then, the two fixed pendulums were released from 90° to determining moment of inertia of the bottom pendulum and the coefficients of friction between bottom pendulum and the cart. Second, the bottom pendulum was fixed, and the top pendulum was released from 90° to determining moment of inertia of the top pendulum and the coefficients of friction between bottom pendulum and the top pendulum.

As a result of the tests, the change of the pendulum angle over time was experimentally measured and recorded. Besides, simulation model was prepared based on (24). By comparing the results from the experiments and also the simulations for two experiments, the coefficients of friction were estimated by using simplex search method in MATLAB (MathWorks, Inc., Natick, MA, USA) using parameter estimation toolbox. In the first experiment, unknown parameters are determined as $b_1 \approx 0.000565$ N/(rad/s) and $J_1 \approx 0.022962$ Nms^2. In the second experiment, unknown parameters are determined as $b_2 \approx 0.000072$ N/(rad/s) and $J_2 \approx 0.002972$ Nms^2. Also, there is friction force between the cart and the surface, where it is moving on. Since effect of the friction of the cart is small, the viscous friction coefficients at the cart (c) are assumed 0.001 Nms.

In order to achieve the stabilization control of the CPDIP system, optimal control theory was addressed in this paper. The general problem of designing an optimal control law involves minimizing a cost function (J) [24] that is defined as following:

$$J = \frac{1}{2}\int_0^\infty \left(x^T Q x + u^T R u\right) dt, \tag{25}$$

where Q is a positive semi – definite matrix, R is positive definite control weighting matrix. For LQR, optimum control signal should be:

$$u\left(t\right) = -R^{-1}B^T P\left(t\right) x\left(t\right) = -Kx\left(t\right), \tag{26}$$

where *P(t)* is the solution of Riccati equation:

$$PA + A^T - PBR^{-1}P + Q = 0. \tag{27}$$

The feedback gain matrix is calculated as:

$$K = \ R^{-1}B^T P = \left[k_1\ k_2\ k_3\ k_4\ k_5\ k_6\right]. \tag{28}$$

Q and R matrices contain the weighting of the system state variables and the control signal respectively. The solution of the optimization problem depends on the Q and R. By tuning Q and R, the desired controller performance is obtained. In simulation, the system can control with the selection of many different matrices. However, the performance of the controller is limited by physical hardware. Therefore, in practice, the desired controller performance can be achieved by optimizing between system response and control performance after choosing an initial value for the Q and R matrices.

In this paper, reasonable initial values were chosen by Bryson's ule [25], which is based on the maximum acceptable error value of the states and maximum allowable value for the control action. The initial weights for the Q matrix are assigned as:

$$Q_{ii} = \frac{1}{(x_{i\ max})^2},\ i = 1, 2, ., n, \tag{29}$$

where x_{imax} is the maximum acceptable error value for the position of state variable x_i. In the electrical circuit model of CPDIP, the position state variables are the charge stored in capacitors ($q_{c1},\ q_{c2},\ q_{c3}$). For the CPDIP system, assume that the acceptable maximum errors for the charge stored in capacitors are 0.3 C, 0.1 C, and 0.02 C, respectively. Therefore, the weight of the cart is 10, the weight of the first pendulum is 100 and the weight of the second pendulum is 2500 and finally $Q_{ii} = [10\ 100\ 2500\ 0\ 0.1\ 0.1]$. Since the sudden changes in the velocity variables are not desired, their weight is chosen as low as possible. The initial weight for the R matrix is assigned as:

$$R = \frac{1}{(u_{max})^2}\rho, \tag{30}$$

where u_{max} is the maximum voltage allowed to be applied to the motor and it is 10 V in this study. With chosen Q and R, the optimal state feedback gain matrix is computed as $[31.6228 - 154.0841 - 364.6620\ \ 51.1444\ - 35.3161\ \ - 40.3124]$.

After choosing the initial values based on electrical circuit model, gain matrix can be tuned on the CPDIP in real-time. The process of tuning is as follows. Initially the feedback gain matrix is obtained from the selected Q and R weight matrices. After that, it is applied to the system and also, a test procedure is developed for observing of the dynamic control performance of the system. This procedure aims to test the performance of the controller on the system to see the desired behavior in specific initial conditions such as in Figure 3. For instance, if the controller is activated when the initial conditions are [0 –0.3 0.5 0 0 0], the cart and the bottom pendulum angle should move in the positive direction and the top pendulum angle should move in the negative direction as can be seen from figure. By implementing of tests, the controller performance is analyzed under many different initial conditions. Consequently, the weights are tuned according to the behavior of the cart and the pendulums. Finally, as a result of tests on the physical system of the CPDIP, gain matrix is tuned as:

$$K = [31.6228 - 152.2980 - 363.5368\ \ 28.6113\ \ - 40.1372\ \ - 25.3043]. \tag{31}$$

To apply LQR controller to the system all system state variables must be measurable. However, not all state variables of the system can always be measured. In such a case, a state estimator is added to the system. State variables of the CPDIP system are $x = [x\ \theta_1\ \theta_2\ \dot{x}\ \dot{\theta}_1\ \dot{\theta}_2]^T$. In the CPDIP, position variables of the system are measured with encoders. Since velocities can't be measured directly, these variables are estimated using second-order derivative filters[1].

$$H(s) = \frac{{W_c}^2 s}{s^2 + 2\zeta W_c s + {W_c}^2}\quad W_c = 2\pi f_c, \tag{32}$$

where W_c is band width, f_c is cut-off frequency and ζ is damping ratio. Since the behaviors of the cart and the pendulums are different, their bandwidths should be also different. Therefore, the bandwidth is selected $2\pi 10$ rad/s for the pendulums and $2\pi 50$ rad/s for the cart. The damping ratio is chosen as 0.9 for each.

[1]Quanser (2012). Laboratory guide Linear Double Inverted Pendulum Experiment for MATLAB/Simulink Users [online]. Website https://www.quanser.com/products/linear-double-inverted-pendulum/#overview [accessed 10 January 2019]

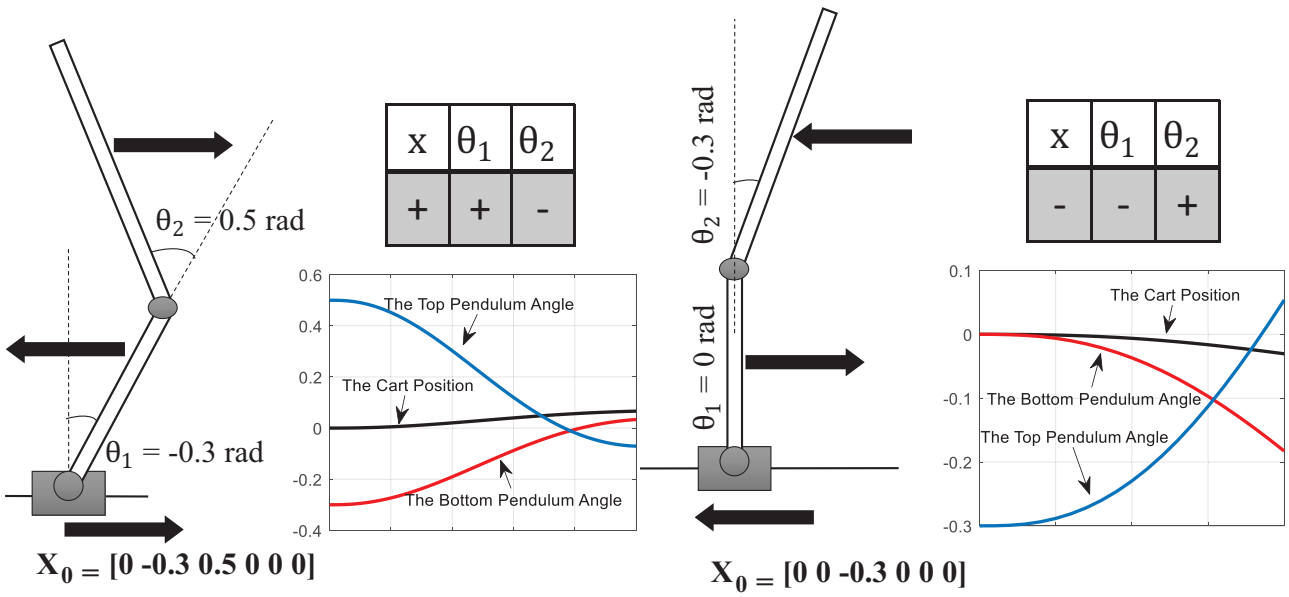

Figure 3. First movement of the CPDIP system under different initial conditions.

4. Experimental results

In this paper, optimal controller was designed for stabilization problem of CPDIP system based on electrical circuit model and the designed controller has been applied to real time experimental setup.

Figure 4 shows the CPDIP control architecture and the experimental setup of the CPDIP system. The CPDIP consists of a cart, two pendulums, a servo motor, three rotary encoders, a belt. The motion of the cart is obtained by the motor connected to the cart by the belt mechanism. MECAPION servo motor with 400W power and MECAPION servo driver in speed mode are used to drive the cart. Analog speed control command is given in the range of [–10V, +10V]. The system mechanism must be durable and robust against the loads and moments to be applied to the system. Each pendulum must be able to rotate 360 degrees freely and there should be no collision between the pendulums during the rotation. The angular positions of the pendulums are measured by the encoder that is mounted the shaft to which the pendulums are connected. The resolutions of the encoders are; 1024 [P/R] for cart position, 1000 [P/R] for the position of the first pendulum and 3000 [P/R] for the second pendulum. dSPACE DS1103 rapid control prototyping system is used to realize experimental applications on the system with a sampling time of $T_s = 1$ millisecond.

Real time LQR Simulink model is shown in Figure 5. In the *Measurement* submodel, the pendulum's angle, and the cart's position are read from encoders. Measured data is filtered by a second derivative filter in 32 and then state feedback controller algorithm is implemented using 31 in *LQR controller* model. Since the encoders start to measure the angles of the pendulums with reference to the point where the pendulums are, the model is initiated when the pendulums are down. Then the pendulums are brought to the upper equilibrium point. At this point, the controller starts to generate the output signal.

The comparison of the simulation and experimental test results of the LQR controller can be seen in Figure 6. As we can see clearly in figure, the controller can successfully stabilize the CPDIP system. Also, Figure 6 shows the consistency of the results of simulation and experimental. If real-time LQR controller

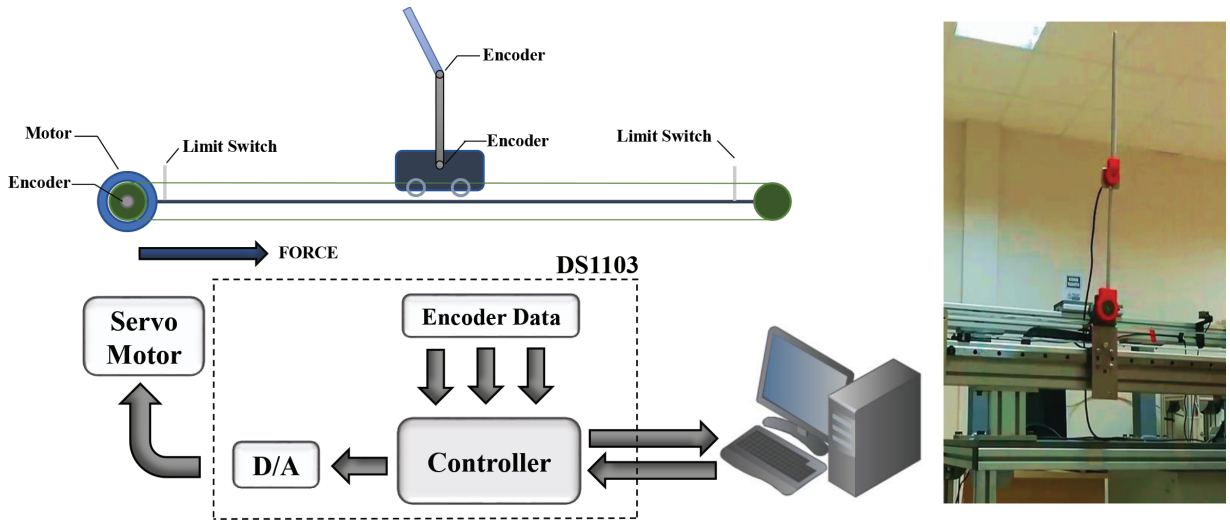

Figure 4. Control structure and the experimental setup of the CPDIP system.

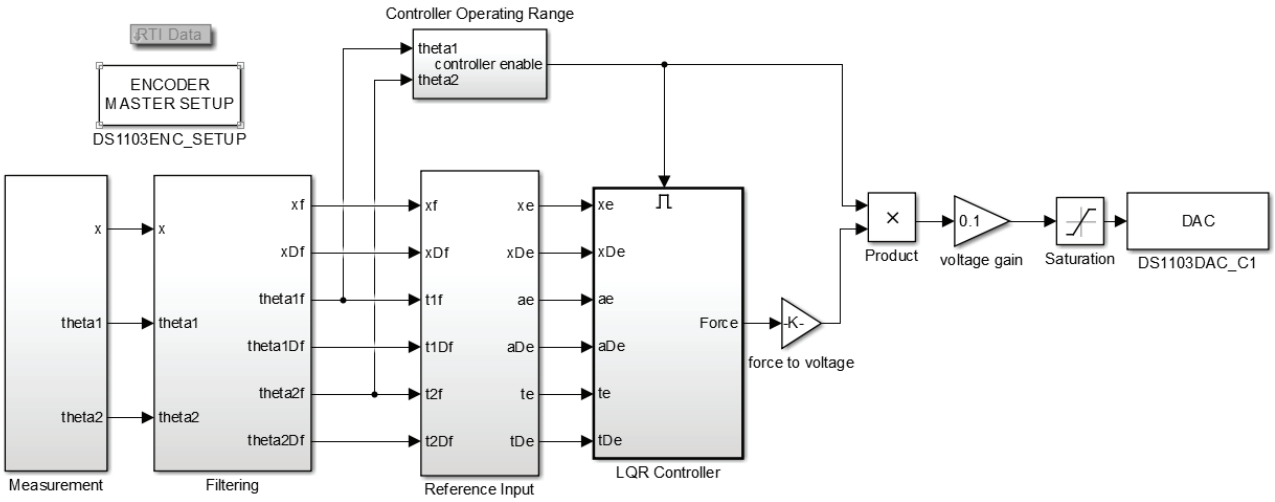

Figure 5. Real time LQR Simulink model.

results are analyzed, we can find that the oscillations of the cart displacement is from –88 mm to –55 mm and pendulums' angles are from –2° to 2.5° and from -1.7° to 0.97°, respectively.

In order to test the robustness and the stabilization performance of the controller in real-time, white noise with variance of 10^{-4} and 10^{-5} are added to the cart position and pendulum positions, respectively. The experimental results of the controller in noisy condition are shown in Figure 7. The oscillation values when measurement noise applied are close to the oscillations shown in Figure 6. In other words, the results obtained with/without measurement noise are approximate. When the data are noisy, the LQR controller maintains the control performance.

For external disturbance test, an impulse signal is added to the control signal applied to the cart (The period of the impulse signal is 4 sec and the amplitude is 1 V). Thus, same disturbing effect on the movement of the cart and pendulums can be obtained. As a result of this test, the LQR controller was able to eliminate

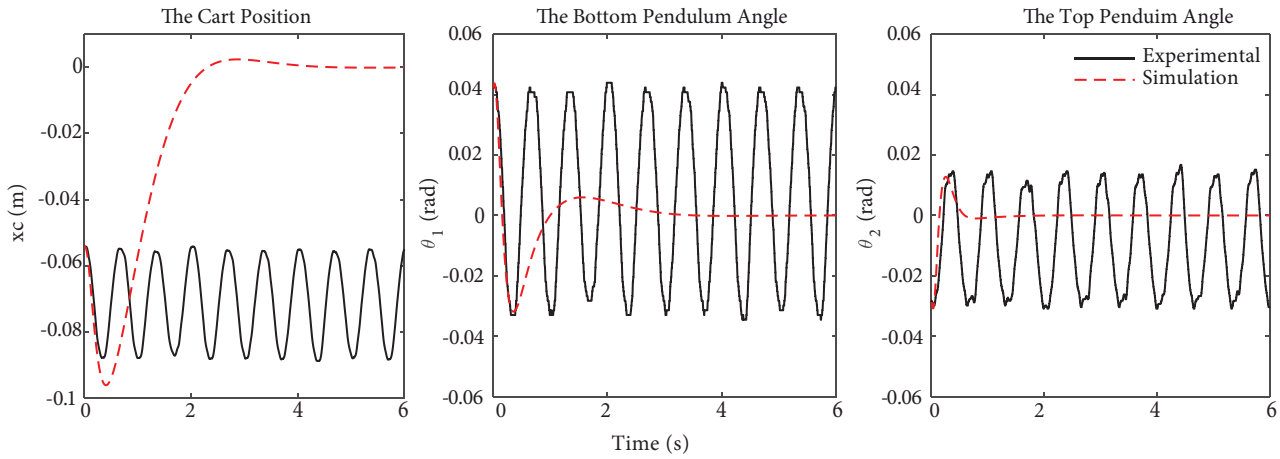

Figure 6. Experimental and simulation results with LQR controller.

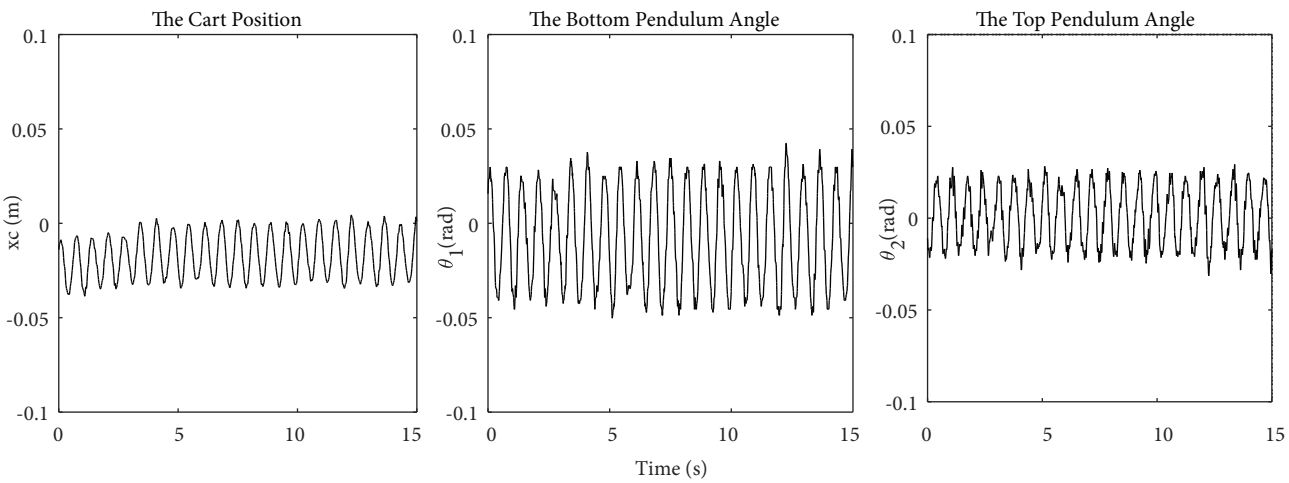

Figure 7. Experimental system outputs in noisy condition.

the disturbing effects and the stabilization of the system is maintained as shown in Figure 8. However, since the disturbance signal is applied to the system periodically, the amount of oscillation in the output variables is greater than that obtained in the tests made in the other conditions.

5. Conclusion

The presented work deals with the power-based modelling and stabilization control of a cart-pole double inverted pendulum. The model of the system is accomplished with an analogy between mechanical and electrical systems that is based on the BM equations. An electrical interpretation of the system is developed and the electrical equivalent circuit of the CPDIP system is obtained. By using the equivalent circuit, a linear quadratic regulator (LQR) controller is designed and implemented on a real time experimental setup. Thus, the controller design of a complex mechanical system is made possible with the basic electrical point of view.

Based on the mathematical model that derived from electrical circuit and the tuning process, the gain matrix consisting of six parameters is determined for the LQR controller in real time. The proposed process

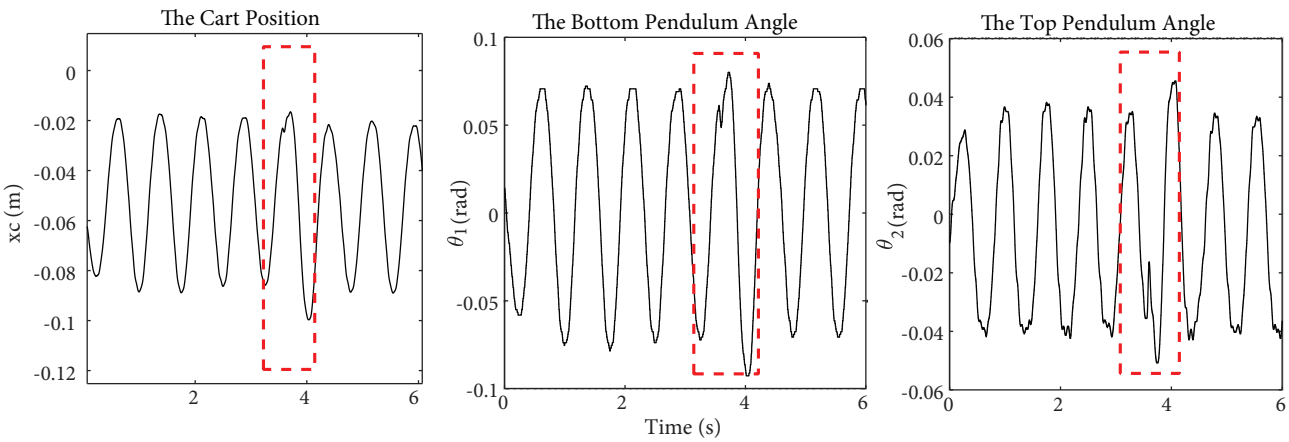

Figure 8. Experimental LQR controller output signals in impulse condition.

is a practical and effective method for the stabilization control of the CPDIP system. Several experiments are conducted in order to test the robustness and the stabilization performance of the controller. LQR controller based on power based modelling is shown to successfully handle the measurement noise and the external disturbances. Experimental results reveal that the Brayton-Moser equations are a convenient and practical alternative to the Lagrangian frameworks.

The proposed electrical equivalent circuit is a special solution that can be used in the modeling of a CPDIP. Through this developed solution, the circuit parameters for any CPDIP testbed can be calculated in a simple way, and the system model can be easily obtained with the basic current-voltage equations. In model-based control studies, taking the circuit proposed for the system model as a reference will save time for the designer and makes it possible to focus more on the development of the controller design.

References

[1] Abraham R, Marsden J. Foundations of Mechanics. Providence, Rhode Island, USA: American Mathematical Society, 2008.

[2] MacFarlane AGJ. Dynamical System Models. London, UK: George Harrap & Co. Ltd.,1970.

[3] Ortega R, Loría A, Nicklasson PJ. Passivity-based Control of Euler-Lagrange Systems; Mechanical, Electrical and Electromechanical Applications. Communications and Control Engineering, London, UK: Springer, 1998.

[4] Jeltsema D, Scherpen JMA. On mechanical mixed potential, content and co-content. In: 2003 European Control Conference (ECC); 2003. pp. 435-440.

[5] Kosaraju KC, Pasumarthy R, Jeltsema D. Modeling and boundary control of infinite dimensional systems in the Brayton-Moser framework. IMA Journal of Mathematical Control and Information 2019; 36: 485-513.

[6] Kosaraju KC, Cucuzzella M, Scherpen JM, Pasumarthy R. Differentiation and Passivity for control of Brayton-Moser systems. IEEE Transactions on Automatic Control 2020; 2 (2): 1-1. doi: 10.1109/TAC.2020.2994317

[7] Brayton RK, Moser JK. A theory of nonlinear networks-I. Quarterly of Applied Mathematics 1964; 22 (1): 1-33.

[8] Dirksz DA, Scherpen JMA. Power-based setpoint control: Experimental results on a planar manipulator. IEEE Transactions on Control Systems Technology 2012; 20: 1384-1391.

[9] Simiyu P, Xin A, Mouhammed N, Kunyu W, Gurti J. Multi-terminal medium voltage DC distribution network large-signal stability analysis. Journal of Electrical Engineering & Technology 2020; 15: 2099-2110.

[10] Zheng H, Zhou L, Sun P, Lu W. Large-signal stability analysis for VSC-HVDC systems based on mixed potential theory. IEEE Transactions on Power Delivery 2020; 35 (4): 1939-1948.

[11] Li Z, Pei W, Ye H, Kong L. Large signal stability analysis for DC microgrid under droop control based on mixed potential theory. The Journal of Engineering 2019; 2019: 1189-1193.

[12] Kosaraju KC, Chinde V, Pasumarthy R, Kelkar A, Singh NM. Stability analysis of constrained optimization dynamics via passivity techniques. IEEE Control Systems Letters 2018; 2 (1): 91-96.

[13] Jeltsema D, Scherpen JMA. Multidomain modeling of nonlinear networks and systems. IEEE Control Systems Magazine 2009; 29: 28-59.

[14] García-Canseco E, Jeltsema D, Ortega R, Scherpen JM. Power-based control of physical systems. Automatica 2010; 46: 127-132.

[15] de Rinaldis A, Scherpen J. An electrical interpretation of mechanical systems via the pseudo-inductor in the Brayton-Moser equations. In: Proceedings of the 44th IEEE Conference on Decision and Control; 2005. pp. 5983-5988.

[16] Jeltsema D, Scherpen JM. A power-based description of standard mechanical systems. Systems & Control Letters 2007; 56 (5): 349-356.

[17] Odry, Á, Burkus E, Odry P. LQG Control of a two-wheeled mobile pendulum system. In: The Fourth International Conference on Intelligent Systems and Applications; 2015. pp. 105-112.

[18] Glück T, Eder A, Kugi A. Swing-up control of a triple pendulum on a cart with experimental validation. Automatica 2013; 49: 801-808.

[19] Graichen K, Treuer M, Zeitz M. Swing-up of the double pendulum on a cart by feedforward and feedback control with experimental validation. Automatica 2007; 43: 63-71.

[20] Zhang J, Zhang W. LQR self-adjusting based control for the planar double inverted pendulum. Physics Procedia 2012; 24: 1669-1676.

[21] Chen X, Yu R, Huang K, Zhen S, Sun H et al. Linear motor driven double inverted pendulum: a novel mechanical design as a testbed for control algorithms. Simulation Modelling Practice and Theory 2018; 81: 31-50.

[22] Yaren T, Kizir S, Yıldız AB. Electrical equivalent circuit based analysis of double pendulum system. In: 2019 6th International Conference on Electrical and Electronics Engineering (ICEEE); 2019. pp. 258-262.

[23] Alexander CK, Sadiku MNO. Fundamentals of Electric Circuits. New York, NY, USA: McGraw Hill Higher Education, 2008.

[24] Bogdanov A. Optimal Control of a Double Inverted Pendulum on a Cart. CSEE, Hillsboro, OR, USA: The OGI School of Science and Engineering, 2004.

[25] Li B. Rotational double inverted pendulum. MSc, University of Dayton, Ohio, United States of America, 2013.